Chemical Papers (2023) 77:7539–7549
https://doi.org/10.1007/s11696-023-03043-4

ORIGINAL PAPER

Study the corrosion issues on galvanized steel induced in water tanks

Ghalia A. Gaber[1] · **Lamiaa Z. Mohamed**[2] · **Aliaa Abdelfatah**[2]

Received: 2 July 2023 / Accepted: 17 August 2023 / Published online: 1 September 2023

Abstract
Weight loss, potentiodynamic polarization, and cyclic voltammetry tests were employed to assess the effects of sodium hypochlorite concentration and pH on the corrosion characteristics of galvanized steel in water tanks. Pitting corrosion appeared on the galvanized steel concurrently in neutral drinkable water. Passivation developed after exposure to 70 mg/L sodium hypochlorite solutions. The results demonstrated that adding NaClO to wastewater solutions reduced the corrosion rate. The corrosion rate of wastewater is 568.7 m/y, which can be reduced by adding NaClO to a lower value of 22.94 m/y at 70 mg/L. NaClO has the maximum efficiency at 70 mg/L, with a value of 95.96%. It was discovered that the galvanized steel in potable water was sensitive to passivation dissolution when hypochlorite solutions with concentrations ranging from 30 to 70 mg/L were added. However, hypochlorite solutions with concentrations greater than 150 mg/L cause significant corrosion on galvanized steel. The PDP and cyclic voltammetry findings revealed that the galvanized steel had good passivation properties under high 70 mg/L sodium hypochlorite concentrations. Only the sodium hypochlorite decreased the amounts of all sessile microorganism families. The scanning electron microscope was employed to check the corroded samples' morphology. Pitting corrosion was discovered alongside galvanic corrosion and uniform corrosion.

Keywords Corrosion · Corrosion measurements · Galvanized steel · Environmental impact · Biocide hypochlorite

Introduction

Buildings, auto body components, and systems for distributing water all require galvanized steel (GS). The Zn coating protects its barrier and galvanic double-protecting activity (Liu et al. 2012). In a humid and wet environment, Zn is anodic to Fe and acts as a sacrificial element (Kartsonakis et al. 2012). However, multiple cases of severe galvanized pipe and tank damage have been related to corrosion methods used in water-hanging networks, as indicated by the formation of rust layers in those structures after an unusually short lifespan (Yadav et al. 2007). Corrosion product accumulation would influence processes involved in corrosion, like oxygen-dissolved, mass transfer, dissolved metal ion hydration, and Zn coating passivation properties. Corrosion products have a considerable impact on metal corrosion resistance.

Fe-tank corrosion in a distribution structure can result in soluble Fe components or Fe-bearing scale loss. The corrosion products can form enormous tubercles, which raise head loss and reduce water capacity. Water's soluble or particulate Fe corrosion byproducts reduce its visual quality and frequently result in customer complaints of "red water" at the tap (Azmat et al. 2011).

Each physical, chemical, and biological factor affecting water distribution systems impacts Fe water tank corrosion, a complex process. Previous research on Fe pipe corrosion has concentrated on several elements of Fe corrosion, including pipe deterioration as assessed by weight loss (WL) or electrochemical, scale development, and byproduct removal as determined by the Fe concentration, color, turbidity, or complaints of the number of customers. For example, one study discovered that head loss increased when pH increased (McNeill and Edwards 2001). However, another study found that increased pH inhibited the release of Fe byproducts. Higher pH may account for more integration of corrosion byproducts within the scale. Still, from the effectiveness

✉ Lamiaa Z. Mohamed
lamiaa.zaky@cu.edu.eg

[1] Department of Chemistry, Faculty of Science (Girls), Al-Azhar University, Yousef Abbas Str., P.O. Box: 11754, Nasr City, Cairo, Egypt

[2] Mining, Petroleum, and Metallurgical Engineering Department, Faculty of Engineering, Cairo University, Giza 12613, Egypt

standpoint, the first consequence is negative, while the second is excellent (Wojtkowska et al. 2022).

Microbes exist in numerous distribution systems and can affect Fe corrosion in a variety of manners (Tong et al. 2019; Le Chevallier et al. 1993). Bacteria were discovered in Fe tubercles. Although bacterial biofilm development on the pipe edge might be a corrosion barrier, biofilms can also generate an altered aeration cell, indicating localized variations in oxygen content and electrical potential. Soluble metals might be taken up through the biopolymers in the biofilm. Numerous bacteria can affect Fe species by reducing Fe^{+3} or oxidizing Fe^{+2}. Bacteria can absorb oxygen, produce corrosive metabolites like H_2S and Fe phosphide, and induce localized pH gradients. Therefore, the function of biological activity in a water line is ambiguous, although it is widely thought to be deleterious to Fe corrosion. In circumstances when activity is prominently led to contain biocides like chlorine, despite their oxidative qualities, efficiently minimize overall corrosion concerns (Minno et al. 2013; De Araujo-Jorge et al. 1992).

Biofilms may have the opposite influence on metal marine corrosion, accelerating or inhibiting degradation (Oliveira et al. 2016). The action of the barrier of biofilm layers that covers the surface of metal uniformly is usually responsible for the reduced corrosion rate (CR). However, biofilms do not cover the metal surface equally, leading to faster corrosion. The anodic and cathodic zones permanent separation, the deterioration products' protective layers collapse, and the anodic or/and cathodic processes stimulation all contribute to this acceleration. Surface colonization and biofilm growth begin when a metallic surface is immersed in water (Telegdi et al. 2020). Biofouling is the unwanted occurrence of adhesion and layers of biofilm built up on an immersed or in link with seawater surface. Several techniques have been employed to reduce the biofouling built up on surfaces, including chemical treatments, such as the biocides in fluids addition for eliminating organisms that gain entry into the system or reducing the growth rate of microorganisms inside the layers, and mechanical methods, like the usage of pigs for eliminating biofilms from systems (Khan et al. 2022). Accessibility, microorganism type, procedure thermal–hydraulic circumstances, treatment costs, safety standards, and environmental concerns influence the method used (Murthy 2004). The main antifouling chemical techniques are the following: chlorination, ozonization, bromochlorination, hydrogen peroxide furthermore, non-oxidizing biocides, synergetic chemical compounds, antifouling coatings, and non-toxic films (Videla and Herrera 2005; Eguia et al. 2008).

Many governmental facilities, such as pools and water-treatment plants, necessitate periodic repair due to chlorine-induced corrosion of their metal components, resulting in high costs and a potential threat to the population's safety (Costa et al. 2023). Although chlorine and sodium hypochlorite (NaClO) appear identical in that both are employed to disinfect water, there are considerable variances, particularly in the amounts utilized in the industry (Ko et al. 2022). Consequently, chlorine is used as a water treatment solution for neither utilization by individuals nor swimming pools (Zhao et al. 2022). It additionally serves as a raw ingredient in the manufacture of sodium hypochlorite (Kamel et al. 2022). Sodium hypochlorite is used in disinfectant manufacturing, and it is available in liquid form, with a 10% to 15% Cl (Grunert et al. 2018).

Chlorination is an established way of preventing biofilm growth in utilities and the manufacturing industry (Telegdi et al. 2020). Since chlorine is transported through the biofilm via managed diffusion, the procedure rate is determined by the chlorine content in the fluid and the system turbulence as a whole (Khan et al. 2022). The chlorine present in the environment has the potential to inactivate microbial cells and oxidize nutrients. Chlorine combines organic and inorganic biofilm components, restricting cell material and inactivating cells. Chlorine may additionally act with the exopolysaccharides (EPSs) that are the main task for the biofilm's integrity in an established biofilm (Khan et al. 2022). Because of the difficulties of biocide absorption into biofilms, eliminating sessile bacteria using biocides is more challenging than killing these germs in circulation (Zuo 2007). Biofilms developed by EPS-rich bacteria require a greater chlorine content than biofilms created by cells that have reduced EPS concentrations (Khan et al. 2022). The hypochlorite deteriorates the EPSs inside the biofilm, causing depolymerization, collapse, and separation of the EPSs (Khan et al. 2022). A sodium hypochlorite solution was employed in this study to reduce the rust coating in the water tanks. Chemical and electrochemical measurements, including WL, PDP, and CV curves, were used to investigate the impacts of pH and Cl^- concentrations on the corrosion manners of GS. Scanning electron microscopy (SEM) was hired to analyze the surface morphologies of the degradation.

Experimental work

The chemical composition of GS utilized for this investigation was first determined using spectrometry. The main constituents of GS are 0.0633% C, 0.0253% Si, 0.164% Mn, and the balance is Fe % in wt%. The Zn covers the outer layer. Studies were conducted in real-world tap water sources. The water sample was collected from Al-Azhar University's Faculty of Science (Girls) lab, which used it as a corrosive environment for GS. The compositions of real tap water were as follows: 65.7 mg/L $NaHCO_3$, 5.75 mg/L KCl, 123.0 mg/L $MgSO_4{\cdot}7H_2O$, and 294.0 mg/L $CaCl_2{\cdot}2H_2O$, pH 7.5, which adjusted by 1 M HNO_3 (65% concentration

from Sigma Aldrich). Surface disinfection of water services, which include water wells, necessitates evaluation to eliminate pathogens from the walls to maintain high-quality drinking water; however, a lot of these procedures may increase corrosion of the contact surfaces and have a negative impact on the circumstances because of disinfectant-polluted waste sludge and wastewater (WW). Almost all therapies nowadays depend on hypochlorite. Passivity inhibitors (passivates) were employed to prevent corrosion in the infrastructure of water-treatment plants. Passivation is the employment of chemicals to interact directly with the minerals in the water flowing into a treatment facility. Passivity inhibitors, often known as disinfectants, included hypochlorite, chlorine dioxide, and chlorine gas. The disinfectants utilized were sodium hypochlorite NaClO from Sigma-Aldrich, and they possessed several different properties: The chlorine level ranges from 4 to 6%, with a specific mass of 1.1 g/mL. The corrosion studies were conducted in hypochlorite aqueous solutions, including 30, 40, 50, 60, and 70 mg/L active chlorine. A hypochlorite ion OCl^- concentration describes active chlorine or free chlorine (Romanovski et al. 2020). The amount of corrosion during GS treatments at appropriate temperatures of sodium hypochlorite for drinking water preparation was examined using WL, electrochemical, and surface analytical methods.

Chlorine bleaching is used to sterilize the water. To do this, the water company combines a dilute solution of sodium hypochlorite (NaClO) with the water, ensuring a continued disinfection impact up to the drinking water delivery point. For compliance with domestic drinking water laws, perfect dosing of the chlorine solution is critical.

The WL experiments were carried out in breakers containing WW solutions of varying pH and sodium hypochlorite NaClO (30–70 mg/L) concentrations at room temperature (RT). Before the tests were performed, the GS specimens were examined. To estimate the WL, the samples were separated from the test solutions after about 30 days of immersion, and the layer of rust was removed with a surgical blade. The rust still on the specimens was removed by covering them in NH_4Cl solution (100 g/L) at 70 °C for 5 min, then washed, dried, and weighed to assess their WL. To evaluate the repeatability of the findings, triplicate specimens were submerged in a glass beaker containing 25 mL of sodium hypochlorite NaClO (30–70 mg/L)-free WW solutions.

Electrochemical experiments were performed in a three-electrode cell with a Pt counter-electrode (Hach Company Radiometer Analytical M23Pt Metal Electrode platinum wire sensor 0.05 mm), a saturated calomel electrode (SCE) as the reference electrode (Glass Body Calomel Reference Electrode 4 mm banana connector, HI1110B, HANNA instruments made in Romania) and a working electrode with surface area 2 cm^2. The most potential in the present work is in SCE units with a cell capacity of 50 ml. The PDP curves were obtained by automatically altering the electrode potential with a PGZ301 potentiostat at a scan rate of 0.5 mV/s between − 1.5 and + 1.0 V. The operational electrode was submerged in the experiment media for 30 min before the corrosion experiment to produce a quasi-stationary assessment of the open circuit potential (OCP). All the investigations were carried out at RT. Equation 1 was used to compute the surface inclusion degrees (θ) in PDP data (Gaber et al. 2020a; b).

$$\theta = 1 - I_{corr}/ I^{\circ}_{corr} \quad (1)$$

where I_{corr}° and I_{corr} donate densities of corrosion current without/with sodium hypochlorite NaClO, respectively.

The following equation was used to calculate the inhibitive efficiency (IE %) (Gaber et al. 2020a; b):

$$IE\ \% = \theta \times 100 \quad (2)$$

The cyclic voltammetry (CV) graphs were displayed by beginning scanning electrode potential at 250 mV under the OCP and progressing to 0 V. Potentials were scanned back to the original potential when the electrode potential approached the anodic potential of 0 V. The vertex current density was set at 0.001 A/cm^2. Electrochemical investigations were performed to assess and examine corrosion using Voltalab 40 Potentiostat PGZ301 (Germany) and Volta Master 4 software.

Scanning electron microscopy (SEM) (model JEOL, model 6460) was employed to analyze the morphology of the specimen surfaces due to corrosion. The coupons were tested before and after the addition of sodium hypochlorite NaClO.

Results and discussion

WL measurements

Effect of concentration of NaClO

The WL of GS in WW solution, after 30 days covering at RT, were taken and illustrated in Fig. 1. Table 1 exhibits the gravimetric corrosion of GS in WW, including several concentrations of NaClO. The CR of GS decreased from 0.0727 to 0.0277 mm/y with the increase of concentration of NaClO from 30 to 70 mg/L. The rising inhibition efficiency implies that the GS surface covering improves by raising NaClO content. Surface coverage θ and IE% increased as the concentration of NaClO was raised, with IE% (64.07) taking place at 70 mg/L of NaClO. Raising the concentration of the tested material in the solution increased the purification effectiveness.

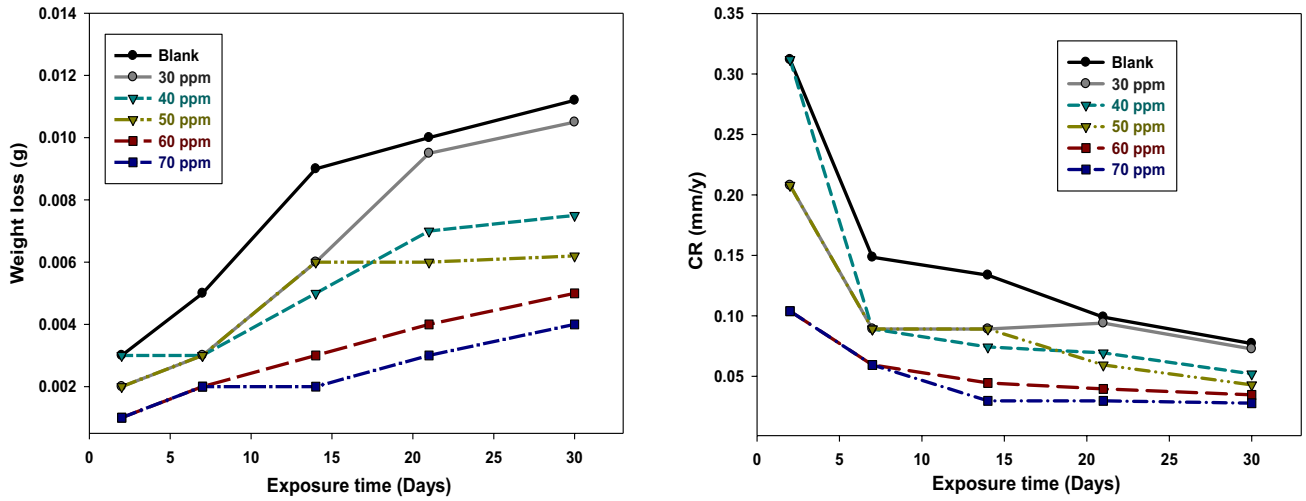

Fig. 1 Variation in WL plots and CR over time for GS at 25 °C with/without various concentrations of sodium hypochlorite NaClO (30–70 mg/L)

Table 1 Corrosion parameters of GS in WW solution with and without various concentrations of NaClO after immersion 30 days

Solutions	Conc. (mg/L)	C_R mm/y	θ	IE (%)
WW	0.0	0.077	–	–
	30	0.073	0.057	5.71
	40	0.052	0.326	32.55
NaClO	50	0.043	0.444	44.35
	60	0.035	0.551	55.12
	70	0.028	0.641	64.07

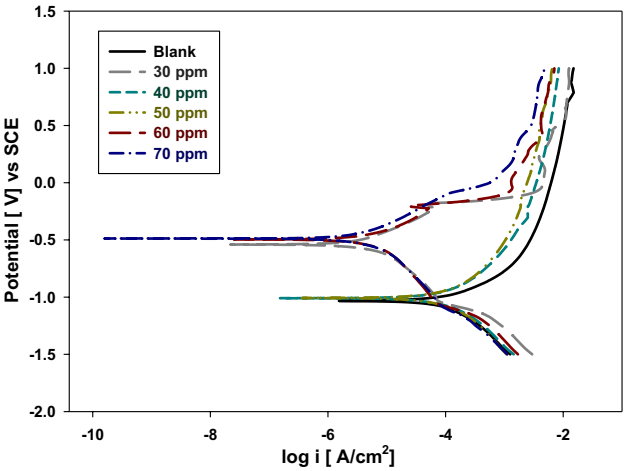

Fig. 2 The PDP curves for GS in WW with different concentrations of NaClO (30–70 mg/L) at 25 °C

Impact of the immersion period

Figure 1 illustrates the variation in WL and CR of GS in WW solution over time with and without NaClO. The graph shows that WL grew as immersion duration increased, although it was smaller in the presence of the examined solutions than in the presence of the WW solution. The amount of time the pipe has been exposed significantly impacts its corrosion. When a pipe is first in contact with water, the Fe content and the CR grow with time, but both eventually decrease as the scale forms. Nevertheless, the specific location of this crossover point varies widely based on the cleanliness of the water and other circumstances (McNeill and Edwards 2001). It was also observed that CR values decreased with an increase in exposure time. Also, the CR of GS is observed to be high with free available hypochlorite, as indicated in Fig. 1 and Table 1. Biofilms may have the opposite impact on metal seawater corrosion, accelerating or inhibiting corrosion. The lowered CR is usually caused by a "barrier" of the deposited biofilm, which covers the surface of metal equally but is not used. It is commonly used for accelerated corrosion. Anodic and cathodic zones permanent separation, the collapse of corrosion products' protective layers, and the stimulation of anodic or cathodic processes, or both, all contribute to this acceleration. The WL vs. time gives a linear relation indicating no insoluble surface coating through corrosion. Furthermore, NaClO was first absorbed into the GS surface and impeded corrosion (Abbas et al. 2022). The findings showed an encouraging increase in IE% when NaClO was applied.

Potentiodynamic polarization estimations

Figure 2 studies PDP plots for the corroded GS in WW with different concentrations of NaClO (30–70 mg/L) at 25 °C. The values of corrosion potential E_{corr}, I_{corr}, cathodic besides anodic Tafel slope (βa and βc), CR, and IE% are recorded in Table 2. Outcome results indicate that upon adding NaClO to WW solutions, the I_{corr} and the CR were reduced. The CR of WW is 568.7 µm/y and is reduced by adding NaClO, attaining a lesser value of 22.94 µm/y at 70 mg/L. The highest efficiency appears in NaClO at 70 mg/L, which values ~ 95.96%. These outcomes coincided well with the WL assessment.

The existence of the oxidized Fe or other compounds deposition onto a corrosion product, which acts like a massive store of corrosion byproducts, the CR of the GS has no link to the quantity of Fe that inter the water. Fe scale is often made up of various chemicals, making it exceedingly uneven. This scale film may offer passivation by restricting oxygen passage to the metal surface and reducing corrosion, but the scale added Fe to the water. This contains soluble scale-dissolving species like scale particles removed from the surface. Predicting solubility is problematic since the scales are frequently weakly crystallized and uneven; even though solubility is understood, the water may be undersaturated due to kinetic or mass transfer constraints. The typical household bleaching agent, liquid sodium hypochlorite (NaOCI), deteriorates inside the biofilm, leading to EPS depolymerization, dissolution, and separation (Khan et al. 2022). The corrosive impact of sodium hypochlorite is caused by producing a high conductivity essential in the electrochemical corrosion mechanism (Zhang et al. 2020). The ability of water to dissolve oxygen constantly reduces as the concentration of NaClO increases, which describes how the CR drops in many circumstances at high concentrations of NaClO (Su et al. 2014).

Romanovski et al. (2020) investigated hypochlorite treatment caused by the maximum Icorr at 150 mg/L active chlorine. Compared to simulated tap water containing 150 mg/L active chlorine, the I_{corr} in calcium and sodium hypochlorite solutions was 4.1 and 3.9 times greater, respectively. Instead, 250 mg/L active chlorine hypochlorite media gives lower I_{corr} than 150 mg/L media, possibly due to a high passivation or pH value.

Cyclic voltammetry measurements

The CV measurements were performed to assess the corrosion resistance of GS in WW with various concentrations of NaClO. The CV approach at a low scan rate was one of the methods used to determine GS's vulnerability to passive stability. Susceptibility to corrosion might be accurately anticipated from the anodic part (Gaber et al. 2020a, b).

Figure 3 demonstrates the CV measurements for GS in WW with different concentrations of NaClO (30–70 mg/L) at 25 °C. The CV plots extract the E_{corr}, E_{pitt}, E_{prot}, and CR listed in Table 3. Overall, the area of the hysteresis loop in CV plots directly relates to the degree of localized corrosion. A big hysteresis loop, for example, suggests that the substance is more prone to corrosion. The area under the loop, which represents the chance of pitting corrosion (PC) occurring, is smaller in the 70 mg/L hypochlorite than in free hypochlorite. The CV confirmed the previous results obtained from WL and PDP examinations. Figure 4

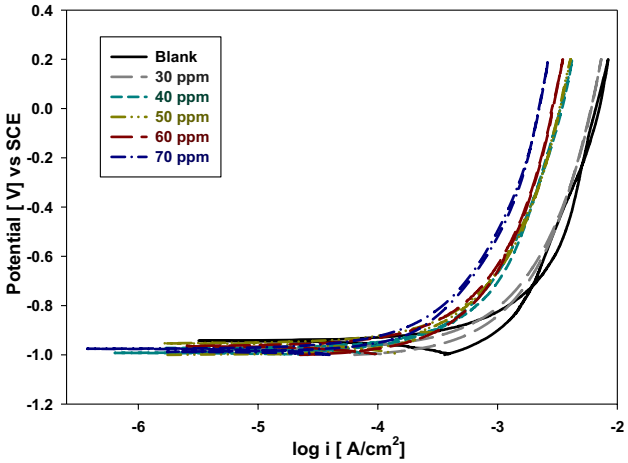

Fig. 3 The CV plots for GS in WW with different concentrations of NaClO at 25 °C

Table 2 Corrosion parameters of the PDP curves for GS in WW with different concentrations of NaClO (30–70 mg/L) at 25 °C

Conc. (mg/L)	E_{corr} mV	I_{corr} µA/cm^2	β_a mV/dec	β_c mV/dec	CR µm/y	θ	IE %
WW	− 1039.0	48.63	132.9	− 187.0	568.7	–	–
30	− 1015.9	42.26	170.0	− 168.1	494.2	0.13	13.10
40	− 1013.8	40.69	169.1	− 178.4	475.8	0.16	16.34
50	− 501.9	2.92	153.9	− 190.7	34.1	0.94	94.01
60	− 545.5	2.38	180.4	− 133.4	27.8	0.95	95.12
70	− 493.9	1.96	165.4	− 149.8	22.9	0.96	95.96

Table 3 Characteristic corrosion parameters from CV for GS in WW with different concentrations of NaClO

Conc. (mg/L)	E_{corr} (V/SCE)	E_{pit} (V/SCE)	E_{prot} (V/SCE)	CR mm/y	θ	IE %
WW	– 0.938	0.138	– 1.00	2.75	–	–
30	– 0.974	0.174	– 0.98	2.15	0.22	21.99
40	– 0.992	0.176	– 0.94	2.10	0.24	23.55
50	– 0.956	0.158	– 0.99	1.17	0.58	57.57
60	– 0.954	0.208	– 0.98	1.13	0.59	58.99
70	– 0.960	0.191	– 0.94	0.91	0.67	67.03

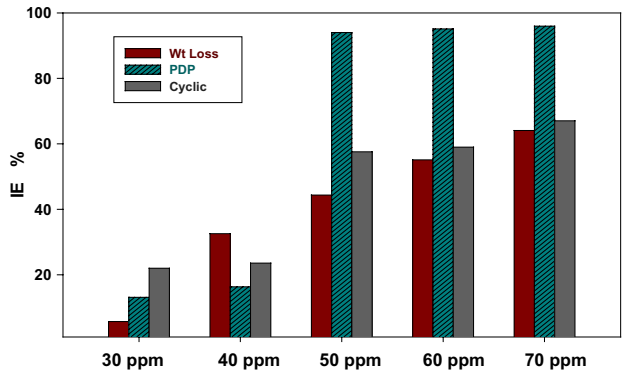

Fig. 4 Comparison IE % with different concentrations of NaClO by WL, PDP, and CV tests

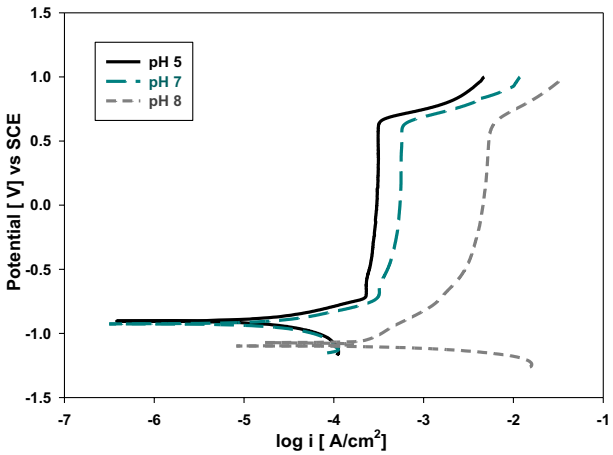

Fig. 5 The PDP curves of GS under different pH values in WW at 60 mg/L NaClO

establishes the IE % for GS in WW with different concentrations of NaClO.

Accordingly, the highest pitting resistance was obtained from the 60–70 mg/L hypochlorite. Hypochlorite shields the GS from pitting corrosion and keeps the layer passive across a broad potential range. This established better performance where the hysteresis loop was noticed throughout the reverse anodic scan, which means that PC may have diminished. Furthermore, the CR has been estimated using the Tafel curve method. From Tafel analysis, GS in free hypochlorite showed a high CR of 2.751 mm/y and was found to be markedly lowered by about 0.907 mm/y in 70 mg/L hypochlorite. The CR values for the GS were high. The high levels of CR were produced by the process's high rate of fluid movement, which caused significant turbulence and corrosion. Biocides, when added to industrial or laboratory environments, diminish or destroy the presence of microbiota. However, they usually raise or slightly lower the system's corrosion rate (Oliveira et al. 2016). Previous investigations using sodium hypochlorite revealed that this biocide is as damaging to carbon steel as hydrogen peroxide, another oxidizing biocide. When contrasted with the control promotes, sodium hypochlorite lowered both the number of sessile microorganisms and the steel values for CR in these trials.

Effects of the pH on galvanized steel in WW at 60 mg/L NaClO

The pH, free existing chlorine, and chloride ion concentration all have an impact on the corrosion response in hypochlorite solution. Because the pH of these solutions is neutral or slightly alkaline (7.5–9.0), hypochlorite ion (OCI^-) will be the dominant form of free-accessible chlorine (Gaur 1994). As a result, chloride and hypochlorite ions will regulate corrosion. The PDP curves of GS vs. pH in 60 mg/L NaClO are shown in Fig. 5. The outcomes of this figure showed that the CR steadily reduced as the pH value increased from 5.0 to 8.0, which can be linked to the influence of corrosion products. The CR decreased from 54.36 to 20.39 mm/y as the pH increased from 5.0 to 8.0. Yeomans (Yeomans 2004) observed the formation of a passive layer on the Zn coating in a highly alkaline solution. As a result, a stable passive layer may be created on GS and serve as a corrosive environment protector (Permeh and Lau 2023). Under high alkalinity, the GS exhibits excellent corrosion resistance.

The CV plots for GS vs. pH in 60 mg/L NaClO are shown in Fig. 6. The solid arrows beside the forward indicated potential scan paths and reverse anodic branches. The GS

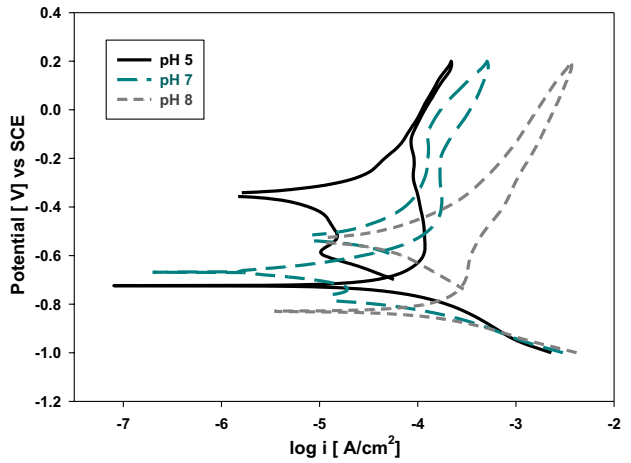

Fig. 6 The CV curves of GS under different pH values in WW at 60 mg/L NaClO

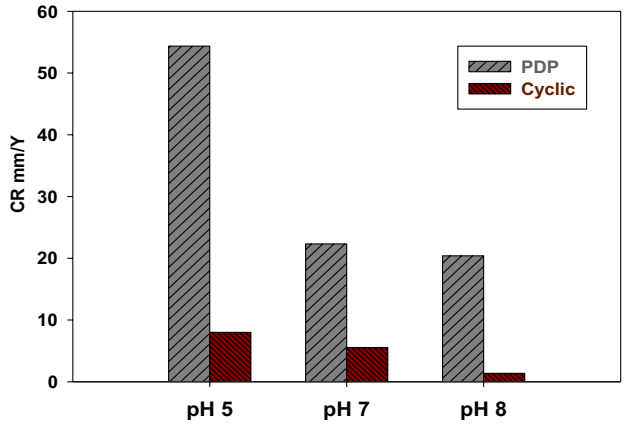

Fig. 7 Comparison effect of pH and CR of NaClO by PDP and CV tests

did not exhibit a conventional passive zone when the pH of the hypochlorite ion (OCI^-) was 7.0. When the pH of hypochlorite ion (OCI^-) was 8.0, the reverse anodic graph illustrated that the pitting potential was practically identical to the OCP, demonstrating that the sample underwent a transition from un-passivated to passivated corrosion behavior. At pH 5.0, Fig. 7 exhibited a characteristic passive area with Icorr nearly independent of applied potential up to pitting potential Epit equal to − 0.649 V vs. SCE. The I_{corr} then climbed quickly until it reached a specific value, following which it grew very slightly with a rise in potential. The reverse anodic graph moved to larger currents than the forward curve while the pH reached 8.0, suggesting that some new corrosion products, maybe a passive layer, were produced on the electrode. At high alkalinity, the $Zn_5Cl_2(OH)_8$ absorbed on the electrode was thermodynamically unstable and prone to the formation of ZnO (Liu et al. 2012). Figure 7 depicts the comparing effect of pH, PDP, and CV. The

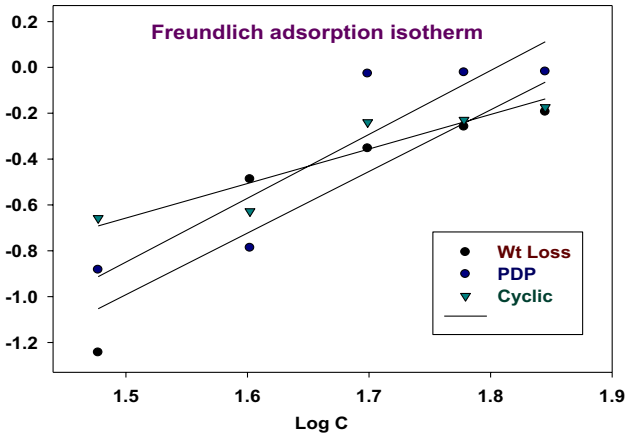

Fig. 8 Adsorption isotherm plots from different measurements for the corroded GS with varying concentrations of NaClO at 25 °C

Table 4 Adsorption parameters on the corrosion of GS with different concentrations of NaClO at 25 °C from different measurements

Technique	R^2	Slope	K_{ads}	ΔG_{ads} kJmol^{-1}
WL	0.83926	2.686363	0.7007	− 9.0713
PDP	0.82227	2.785524	0.7013	− 9.0734
CV	0.85723	1.505969	0.4647	− 8.0553

CR dropped from 8.003 to 1.362 mm/y as the pH increased from 5.0 to 8.0, and GS demonstrated remarkable corrosion resistance in the high alkaline hypochlorite ion (OCI^-). The findings were consistent with the PDP assessment.

Freundlich adsorption isotherm

Adsorption isotherms (AIs) have proved extremely useful in studies involving environmental protection and adsorption strategies. Langmuir and Freundlich are well-known two-parameter AIs. The Langmuir isotherm (LI) is used for homogeneous monolayer adsorption, while the Freundlich isotherm suites are used for heterogeneous multilayer adsorption. Equation 3 shows how, corresponding to the Freundlich isotherm, θ is linked to the concentration C of NaClO (Alahiane et al. 2020).

$$\log \theta = \log K_{ads} + n \log C \tag{3}$$

where n denotes the empirical constant, the other constants have a comparable indication. Figure 8 expressions straight lines are due to $\log \theta$ against $\log C$ with slope n and intercept $\log K_{ads}$. The deduced adsorption parameters K_{ads}, n, and ΔG°_{ads} are displayed in Table 4. It was found the correlation factor values are far from unity. Freundlich isotherms were used to investigate the adsorption process. The adsorption

investigations demonstrated unequivocally that the experimental data suited the Freundlich adsorption isotherms with high linearity. The best-fit isotherm criteria depend on a greater correlation coefficient, R^2.

A perfect linear plot was produced with a regression constant $R^2 = 0.83926$ and a slope of about 1.505969, nearly equal for all techniques used. It is customary that the standard free energy (ΔG_{ads}) evaluated by the subsequent Eq. 4 (Shahen et al. 2022):

$$K_{ads} = 1/55.5 \exp\left(-\left(\Delta G_{ads}/RT\right)\right) \quad (4)$$

The value of ΔG_{ads} is -9.0713 kJ·mol^{-1}, nearly equal for the WL, PDP, and CV tests. This negative number indicates that the adsorption activity is uncontrolled. Furthermore, ΔG_{ads} values at or below -20 kJ·mol^{-1} or less are consistent with the electrostatic interaction of both charged metal and molecules (physisorption) (Shahen et al. 2022). The calculated ΔG_{ads} values are lower negative than -20 kJ·mol^{-1} representing that physisorption is typical of the adsorption development of the NaClO concentration.

Surface morphology

Morphology by SEM images was operated to examine further the corrosion of GS in WW free with and without 60 mg/L NaClO and at different pH values. Figure 9 performs the SEM images of GS in WW free with and without 60 mg/L NaClO. The coatings with Zn were compact, smooth, and coated on the Zn coating surface. The CR values obtained from WL readings are higher. This is to be considered because CR is highest at the start and diminishes with time due to the creation of corrosion products to achieve an equilibrium value. The concentration of free accessible chlorine appears to raise the CR value. The mechanism of corrosion reveals that the exchange Icorr for Fe/$Fe(OH)_z$ and the current density limit for OCl^-/Cl increase with the concentration of free accessible chlorine. These modifications boost the CR with free accessible chlorine. The CR value decreases with 60 mg/L NaClO than blank WW due to the covering of passive corrosion products that cover the test sample than that on blank WW.

However, if the Zn is deposited excessively, increasing surface roughness, the GS may bear from intergranular corrosion. The GS degradation is like conventional steels, but GS exhibits a distinct type of corrosion known as "bimetallic corrosion" or "galvanic corrosion." This sort of corrosion happens owing to a large potential difference between materials, with Zn being a very anodic material that may resist a noble material that is very cathodic. This process is accelerated when the water has a high conductivity (Anaman et al. 2022).

Figure 10 depicts SEM images of the GS immersed in 60 mg/L NaClO at pH 5.0, 7.0, and 8.0. After 30 days in the pH 7.0 solution, the rust layer was absorbed on the surface of the electrode, and PC was located on the electrode interface in the 60 mg/L NaClO solution. The Zn coating began deteriorating after eliminating the rust layer, and non-uniform corrosion developed on GS. Throughout the immersion time, however, a needle-like rust layer was adherent and compactly absorbed on the electrode surface in the pH 8.0 solution, the color of the surface became murky grey, and no pitting was seen on the Zn coating. According to SEM micrographs, passivation happened on GS in a highly alkaline atmosphere. These findings were consistent with the WL experiments. Fe was detected in pH 5.0 and pH 7.0, showing that the Zn coating was harmed by Cl- erosion. Higher pH values increased the oxide content while

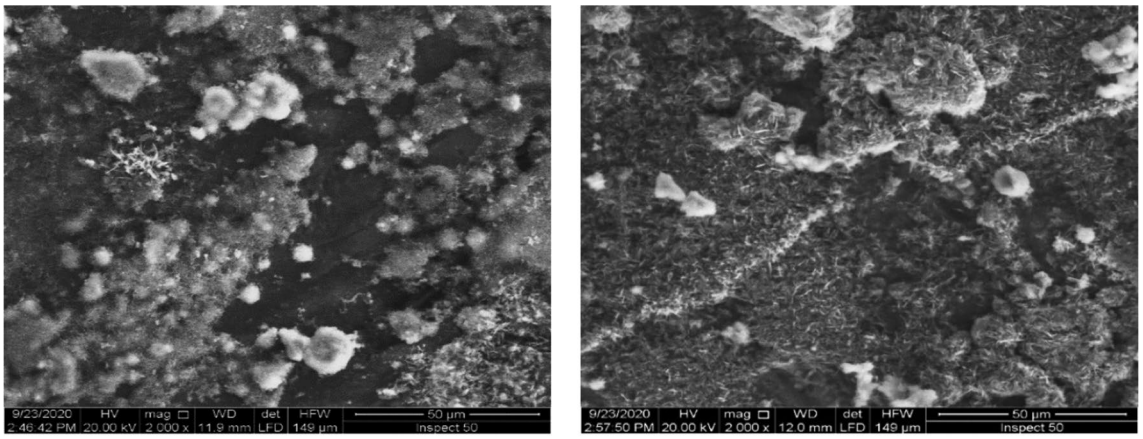

Fig. 9 The SEM images of WW for **a** blank in WW and **b** WW with 60 mg/L NaClO

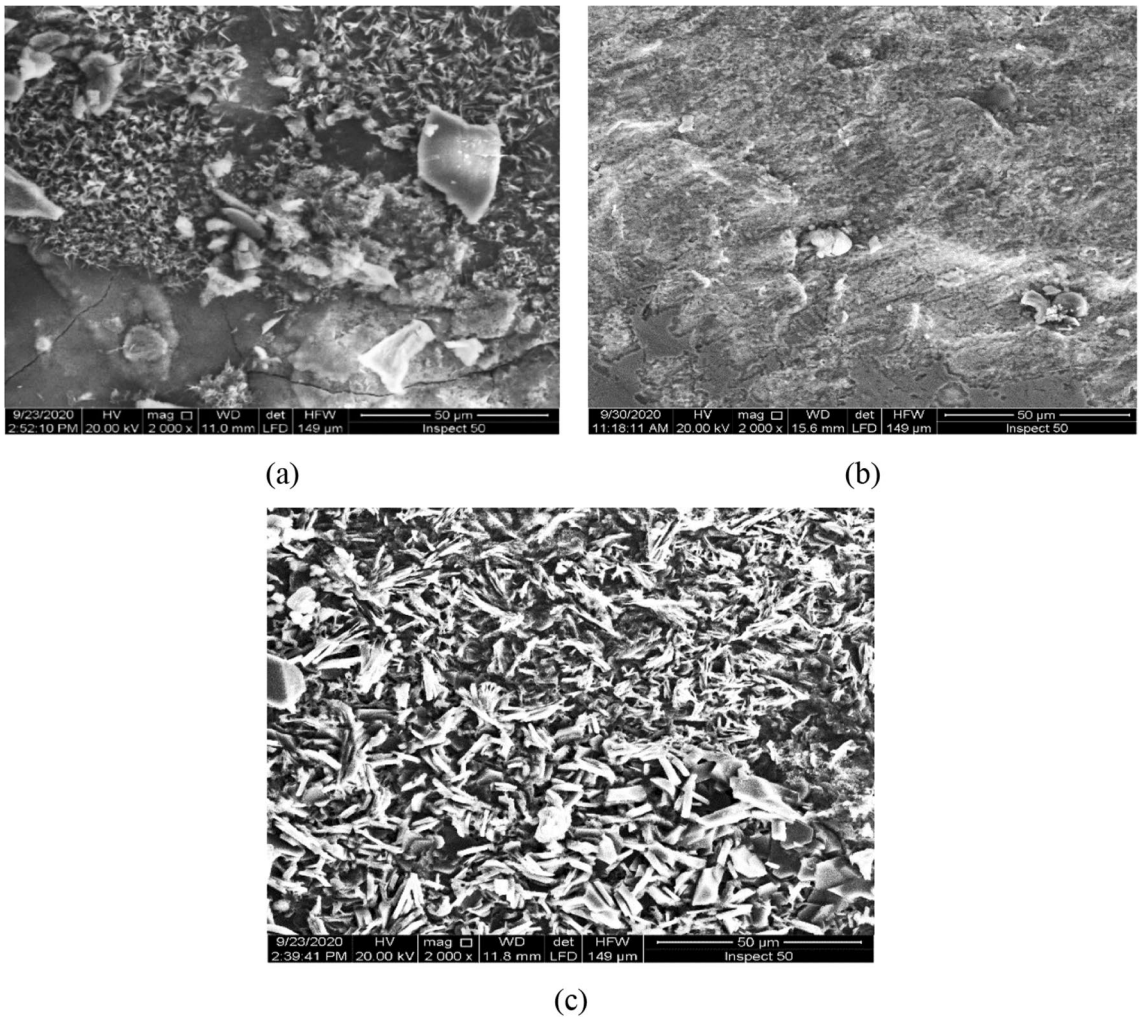

Fig. 10 The SEM images of GS at different pH after 30 days of immersion in 60 mg/L NaClO at pH equal to **a** 5, **b** 7, and **c** 8

the chloride content declined, indicating that Zn oxide was produced in the highly alkaline solution. By increasing the pH of OCl^-, corrosion of GS was prevented. The corrosion product morphology after sodium hypochlorite treatments differed slightly. There were needle-shaped, platelet-shaped, and spherical particles identified, with no discernible difference in composition. The hypochlorite solutions appeared to affect the size and nature of the corrosion deposit. The Na was found in larger concentrations in the corrosion products of the NaClO-treated samples than in the other treated samples. Chlorine was only found in samples previously considered with hypochlorite solutions.

It should be noted that all concentrations have been processed in WW, which contains trace levels of Ca, Na, K, and chlorides, among other things. All surface disinfection-treated samples had cracks and local flaws. Increasing pH values from 5.0 to 7.0 led to containing a protective layer, as shown in Fig. 10. Furthermore, the rise of pH from 7.0 to 8.0 changed the morphology of the corrosion products, and more passivation happened. That matches the CR values from PDP and CV measurements as in Fig. 7.

Conclusion

The research investigations were carried out to examine corrosion difficulties on GS caused by hypochlorite ion concentration in water tanks. Chemical and electrochemical testing were used to study the effect of pH levels and Cl^- concentration on the corrosion characteristics of GS. The following significant findings were reached:

- The CR value of free chlorine content is 568.7 m/y, called blank WW.
- The GS rusted actively in WW, but the most severe corrosion occurred in hypochlorite solutions with concentrations greater than 150 mg/L.

- After surface disinfection with hypochlorite, hypochlorite or chlorine with chemicals were trapped in corrosion species, and cracks were demonstrated to alter the pH in later WW exposure.
- The WL, PDP, and CV curves all indicated that the GS had good passivation in the media tested. Furthermore, the rust coating absorbed on the GS surface may prevent future corrosion.
- The morphology of products due to corrosion by adding sodium hypochlorite addition varied slightly. There were needle-shaped, platelet-shaped, and spherical particles identified, with no discernible difference in composition. There was observed pitting corrosion, galvanic corrosion, and uniform corrosion.

Funding Open access funding provided by The Science, Technology & Innovation Funding Authority (STDF) in cooperation with The Egyptian Knowledge Bank (EKB).

Declarations

Conflict of interest The authors declare that they have no conflict of interest.

References

Abbas MA, Arafa EI, Gad ES, Bedair MA, El-Azabawy OE, Al-Shafey HI (2022) Performance assessment by experimental and theoretical approaches of newly synthesized benzyl amide derivatives as corrosion inhibitors for carbon steel in 1.0 M hydrochloric acid environment. Inorg Chem Commun 143:109758–109778

Alahiane M, Oukhrib R, Albrimi YA, Oualid HA, Bourzi H, Akbour RA, Assabbane A, Nahlé A, Hamdani M (2020) Experimental and theoretical investigations of benzoic acid derivatives as corrosion inhibitors for AISI 316 stainless steel in hydrochloric acid medium: DFT and Monte Carlo simulations on the Fe (110) surface. RSC Adv 10:41137–41153

Anaman SY, Lee S, Cho HH, Hong ST (2022) A comprehensive assessment of the galvanic corrosion behavior of an electrically assisted pressure joint of dissimilar stainless-steel alloys under uniaxial tensile stress. J Mater Res Technol 19:3110–3129

Azmat NS, Ralston KD, Muddle BC, Cole IS (2011) Corrosion of Zn under acidified marine droplets. Corros Sci 53:1604–1615

Costa RDFS, Barbosa MLS, Silva FJG, Sousa SR, Sousa VFC, Ferreira BO (2023) Study of the chlorine influence on the corrosion of three steels to be used in water treatment municipal facilities. Materials 16:2514

De Araujo-Jorge TC, Melo Coutinho CML, De Aguiar LEV (1992) Sulphate-reducing bacteria associated with biocorrosion—A review. Memorias Instituto Oswaldo Cruz 87(3):329

Eguia E, Trueba A, Río-Calonge B, Girón A, Bielva C (2008) Biofilm control in tubular heat exchangers refrigerated by seawater using flow inversion physical treatment. Int Biodeterior Biodegradation 62:79–87

Gaber GA, Aly HA, Mohamed LZ (2020a) Effect of sodium tungstate on the corrosion behavior of Fe base alloy in H_2SO_4 solution. Int J Electrochem Sci 15:8229–8240

Gaber GA, Hussein WA, Ghanem WA (2020b) Nanoparticles deposition effects on 1050A aluminum alloy anodic layers. Mater Res Express 7(1):016567

Gaur B (1994) Corrosion of mild steel in hypochlorite solution-an electro weight-loss study. Indian J Chem Technol 1:225–229

Grunert A, Frohnert A, Selink HC, Szewzyk R (2018) A new approach to testing the efficacy of drinking water disinfectants. Int J Hyg Environ Health 221:1124–1132

Kamel M, El-Ashtoukhy ESZ, Abdel-Aziz MH, Zahran RR, Sedahmed GH, El Gheriany I (2022) Effect of additives and electrode roughness on the production of hypochlorite sanitizer by the electrolysis of NaCl solution in a batch recycle reactor. Chem Eng Process Process Intensif 176:108959

Kartsonakis IA, Balaskas AC, Koumoulos EP, Charitidis CA, Kordas GC (2012) Incorporation of ceramic nanocontainers into epoxy coatings for the corrosion protection of hot dip galvanized steel. Corros Sci 57:30–41

Khan MS, Liang T, Liu Y, Shi Y, Zhang H, Li H, Guo S, Pan H, Yang K, Zhao Y (2022) Microbiologically influenced corrosion mechanism of ferrous alloys in marine environment. Metals 12:1458

Ko KH, Kim GH, Song JG, Kim SG (2022) A novel cyclic voltammetric determination of free chlorine generated by ozone disinfection in seawater aquarium. Chin J Anal Chem 50:100067

Le Chevallier MW, Lowry CD, Lee RG, Gibbon DL (1993) Examining the relationship between iron corrosion and the disinfection of biofilm bacteria. J AWWA 85(7):111

Liu S, Sun H, Sun L, Fan H (2012) Effects of pH and Cl^- concentration on corrosion behavior of the galvanized steel in simulated rust layer solution. Corros Sci 65:520–527

McNeill LS, Edwards M (2001) Review of iron pipe corrosion in drinking water distribution systems. J Awwa 93(7):88–100

Minno B, Ilhan-Sungur E, Çotuk A, Güngör ND, Cansever N (2013) The corrosion behaviour of galvanized steel in cooling tower water containing a biocide and a corrosion inhibitor. Biofouling 29(3):223–235

Murthy PS (2004) Biofilm control for plate heat exchangers using surface seawater from the open ocean for the OTEC power plant. Int Biodeterior Biodegradation 53:133–140

Oliveira SH, Lima MAGA, França FP, Vieira MRS, Silva P, Filho SLU (2016) Control of microbiological corrosion on carbon steel with sodium hypochlorite and biopolymer. Int J Biol Macromol 88:27–35

Permeh S, Lau K (2023) Corrosion of galvanized steel in alkaline solution associated with sulfate and chloride ions. Constr Build Mater 392(15):131889

Romanovski V, Claesson PM, Hedberg YS (2020) Comparison of different surface disinfection treatments of drinking water facilities from a corrosion and environmental perspective. Environ Sci Pollut Res 27:12704–12716

Shahen S, Abdel-karim AM, Gaber GA (2022) Eco-friendly roselle (Hibiscus Sabdariffa) leaf extract as naturally corrosion inhibitor for Cu-Zn alloy in 1M HNO_3. Egypt J Chem 65(4):351–361

Su W, Tian Y, Peng S (2014) The influence of sodium hypochlorite biocide on the corrosion of carbon steel in reclaimed water used as circulating cooling water. Appl Surf Sci 315:95–103

Telegdi J, Shaban A, Trif L (2020) Review on the microbiologically influenced corrosion and the function of biofilms. Int J Corros Scale Inhib 9(1):1–33

Tong H, Li Z, Hu X, Xu W, Li Z (2019) Metals in occluded water: a new perspective for pollution in drinking water distribution systems. Int J Environ Res Public Health 16:2849

Videla HA, Herrera LK (2005) Microbiologically influenced corrosion: looking to the future. Int Microbiol 8:169–180

Wojtkowska M, Malesinska A, Machowska A, Puntorieri P, Barbaro G, Fiamma V, Biedugnis S (2022) The influence of water quality change on the corrosion process in galvanized pipes of fire protection installations. Sustainability 14:7708

Yadav AP, Katayama H, Noda K, Masuda H, Nishikata A, Tsuru T (2007) Surface potential distribution over a zinc/steel galvanic couple corroding under thin layer of electrolyte. Electrochim Acta 52:3121–3129

Yeomans SR (2004) Galvanized steel reinforcement in concrete. Elsevier, Oxford, pp 113–117

Zhang H, Zhao L, Liu D, Wang J, Zhang X, Chen C (2020) Early period corrosion and scaling characteristics of ductile iron pipe for ground water supply with sodium hypochlorite disinfection. Water Res 176:115742

Zhao J, Peng J, Yin R, Fan M, Yang X, Shang C (2022) Multi-angle comparison of UV/chlorine, UV/monochloramine, and UV/chlorine dioxide processes for water treatment and reuse. Water Res 217:118414

Zuo R (2007) Biofilms: strategies for metal corrosion inhibition employing microorganisms. Appl Microbiol Biotechnol 76:1245–1253